Accuracy of Homology based Coverage Hole Detection for Wireless Sensor Networks on Sphere

Feng Yan, Philippe Martins, Laurent Decreusefond

Accuracy of Homology based Coverage Hole Detection for Wireless Sensor Networks on Sphere

Feng Yan, Philippe Martins, *Senior Member, IEEE,* and Laurent Decreusefond

Abstract—Homology theory has attracted great attention because it can provide novel and powerful solutions to address coverage problems in wireless sensor networks. They usually use an easily computable algebraic object, Rips complex, to detect coverage holes. But Rips complex may miss some coverage holes in some cases. In this paper, we investigate homology-based coverage hole detection for wireless sensor networks on sphere. The situations when Rips complex may miss coverage holes are first presented. Then we choose the proportion of the area of coverage holes missed by Rips complex as a metric to evaluate the accuracy of homology-based coverage hole detection approaches. Three different cases are considered for the computation of accuracy. For each case, closed-form expressions for lower and upper bounds of the accuracy are derived. Simulation results are well consistent with the analytical lower and upper bounds, with maximum differences of 0.5% and 3% respectively. Furthermore, it is shown that the radius of sphere has little impact on the accuracy if it is much larger than communication and sensing radii of each sensor.

Index Terms—Wireless sensor networks, coverage hole, homology.

1 Introduction

Wireless sensor networks (WSNs) have attracted considerable research attention due to their wide potential applications such as battlefield surveillance, environmental monitoring and intrusion detection. Many of these applications require a reliable detection of specified events. Such requirement can be guaranteed only if the target field monitored by a WSN contains no coverage holes, that is to say regions of the domain not monitored by any sensor. Coverage holes can be formed for many reasons, such as random deployment, energy depletion or destruction of sensors. Consequently, it is essential to detect and localize coverage holes in order to ensure the full operability of a WSN.

There is already extensive work on the coverage hole problem in WSNs on 2D plane and 3D space. Some of these work used either precise information about sensor locations [1], [2], [3], [4], [5] or accurate relative distances between neighbouring sensors [6], [7], [8] to detect coverage holes. The requirement of precise location or distance information substantially limits their applicability since acquiring such information is either expensive or impractical in many settings. Thus connectivity-based approaches are of great interest for us. In this category, homology-based schemes have received special attention because of its powerfulness for coverage problems in WSNs.

Homology was first introduced by Ghrist and his collaborators in [9], [10], [11] to address the coverage problems in WSNs. They introduced a combinatorial object, Čech complex, which fully characterizes coverage properties of a WSN (existence and locations of holes). Unfortunately, this object is very difficult to construct even if the precise information about the relative locations of sensors is available. Thus, they introduced another more easily computable complex, Vietoris-Rips complex (we will abbreviate the term to Rips complex in this paper). This complex is constructed with the sole knowledge of the connectivity graph of the network and gives an approximate coverage by simple algebraic calculations. More precisely, Rips complex may miss some special coverage holes. It is thus of paramount importance to analyse the coverage holes missed by Rips complex in order to evaluate the accuracy of homology-based coverage hole detection.

The main contributions of our paper are as follows. First, the relationship between Čech complex and Rips complex in terms of coverage hole on sphere is analysed. Furthermore, it is found that a hole in a Čech complex missed by a Rips complex must be surrounded by a spherical triangle. Based on that, a formal definition of spherical triangular hole is given.

Second, we choose the proportion of the area of spherical triangular holes as a metric to evaluate the accuracy of homology-based coverage hole detection. Such proportion is analysed under a homogeneous setting and it is related to the communication and sensing radii of each sensor. Three cases are considered for the computation of such proportion. For each case, closed-form expressions for lower and upper bounds of the proportion are derived.

Third, extensive simulations are performed to evaluate impacts of communication and sensing radii, radius

• *F. Yan, P. Martins and L. Decreusefond are with the Network and Computer Science Department, TELECOM ParisTech, Paris, France. E-mail: {fyan, martins, decreuse}@telecom-paristech.fr*

of sphere on proportion of the area of spherical triangular holes. It is shown that simulation results are well consistent with the analytical lower bound, with a maximum difference of 0.5%, and consistent with the analytical upper bound, with a maximum difference of 3%. Furthermore, simulation results show that the radius of sphere has little impact on the proportion when it is much larger than communication and sensing radii. It further indicates that our analytical results can be applied to more general 3D surfaces.

The rest of the paper is organised as follows. Section 2 presents the related work. In Section 3, the network model and the formal definition of spherical triangular hole are given. Closed-form lower and upper bounds for proportion of the area of spherical triangular holes under three different cases are derived in Section 4. Section 5 compares simulation results and analytical bounds. Finally, Section 6 concludes the paper.

2 Related work

We present the related work in terms of two aspects: coverage ratio analysis and homology-based coverage hole detection.

First, extensive research has been done to analyse coverage ratio in a WSN on 2D plane or 3D surface. In [12], [13], the fraction of the area covered by sensors was analysed. In [14], the authors studied how the probability of coverage changes with the sensing radius or the number of sensors. In [15], a point in a plane is defined to be tri-covered if it lies inside a triangle formed by three nodes, and the probability of tri-coverage was analysed. In [16], the authors proposed the surface coverage model and derived the expected coverage ratio under stochastic deployment on 3D surface. In [17], the expected coverage ratio under stochastic deployment on 3D rolling terrains was derived. Nevertheless, none of these research considers triangular holes. We provided some initial results about the proportion of the area of triangular holes on 2D plane in [18]. In this paper, we aim to extend results in [18] on sphere.

As for homology-based coverage hole detection, De Silva et al first proposed a centralized algorithm that detects coverage hole via homology in [10]. They constructed the Rips complex corresponding to the communication graph of the network and determined the coverage by verifying whether the first homology group of the Rips complex is trivial. Then the above ideas were first implemented in a distributed way in [19]. It is shown that combinatorial Laplacians are the right tools for distributed computation of homology groups and can be used for decentralized coverage verification. In [20], a gossip-like decentralized algorithm for computation of homology groups was proposed. In [21], a decentralized scheme based on Laplacian flows was proposed to compute a generator of the first homology group. But all these homology-based algorithms do not consider the cases that Rips complex may miss some special coverage holes. In this paper, we describe such cases and analyse the proportion of the area of coverage holes missed by Rips complex.

3 Models and definitions

Consider a collection of stationary sensors (also called nodes) deployed randomly on a sphere $\mathbb{S}^2$ with radius R according to a homogeneous Poisson point process with intensity λ. For any two points p_1 and p_2 on $\mathbb{S}^2$, the distance between them $d(p_1, p_2)$ is defined to be the great circle distance, which is the shortest distance between any two points on the surface of a sphere measured along a path on the surface of the sphere. As usual, isotropic radio propagation is assumed. All sensors have the same sensing radius R_s and communication radius R_c on $\mathbb{S}^2$. It means for any sensor located at v on $\mathbb{S}^2$, any point p on $\mathbb{S}^2$ with $d(v, p) \leq R_s$ is within the sensing range of the sensor; and for any two sensors located at v_i, v_j on $\mathbb{S}^2$, they can communicate with each other if $d(v_i, v_j) \leq R_c$. In addition, we assume $R_s \ll R$, $R_c \ll R$.

Before defining the two combinatorial objects, known as Čech complex and Rips complex, it is necessary to give a brief introduction to some tools used in the paper. For further readings, see [22], [23], [24]. Given a set of points V, a *k*-simplex is an unordered set $[v_0, v_1, ..., v_k] \subseteq V$ where $v_i \neq v_j$ for all $i \neq j$, k is the dimension of this simplex. The faces of this *k*-simplex consist of all (*k*-1)-simplex of the form $[v_0, ..., v_{i-1}, v_{i+1}, ..., v_k]$ for $0 \leq i \leq k$. For example, on a sphere $\mathbb{S}^2$, a 0-simplex $[v_0]$ is a vertex , a 1-simplex $[v_0, v_1]$ is the shorter arc of the great circle passing through v_0 and v_1, a 2-simplex $[v_0, v_1, v_2]$ is a spherical triangle $v_0v_1v_2$ with its interior included, see Fig. 1. An abstract simplicial complex is a collection of simplices which is closed with respect to inclusion of faces. A k-dimensional abstract simplical complex $\mathcal{K}$ is an abstract simplicial complex where the largest dimension of any simplex in $\mathcal{K}$ is k.

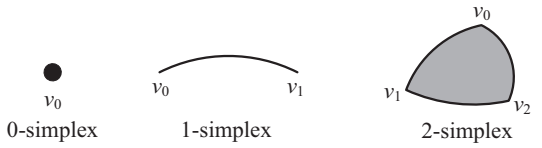

Fig. 1. 0-, 1- and 2-simplex

Let $\mathcal{V}$ denote the set of sensor locations in a WSN on $\mathbb{S}^2$ with radius R and $\mathcal{S} = \{s_v, v \in \mathcal{V}\}$ denote the collection of sensing ranges of these sensors: for a location v, $s_v = \{x \in \mathbb{S}^2 : d(x, v) \leq R_s\}$. Then Čech complex and Rips complex can be defined as follows.

Definition 1 (Čech complex)**.** *Given a finite collection of sensing ranges $\{s_v, v \in \mathcal{V}\}$, the Čech complex of the collection, $\check{C}(\mathcal{V})$, is the abstract simplicial complex whose k-simplices correspond to non-empty intersections of k + 1 distinct elements of $\{s_v, v \in \mathcal{V}\}$.*

Definition 2 (Rips complex)**.** *Given a metric space $(\mathbb{S}^2, d)$, a finite set of points $\mathcal{V}$ on $\mathbb{S}^2$ and a fixed radius ϵ, the Rips complex of $\mathcal{V}$, $\mathcal{R}_\epsilon(\mathcal{V})$, is the abstract simplicial complex whose k-simplices correspond to unordered (k +1)-tuples of points in $\mathcal{V}$ which are pairwise within distance ϵ of each other.*

According to the definitions, the Čech complex and Rips complex of the WSN, respectively denoted by $\check{\mathrm{C}}_{R_s}(\mathcal{V})$ and $\mathcal{R}_{R_c}(\mathcal{V})$, can be constructed as follows: a k-simplex $[v_0, v_1, \cdots, v_k]$ belongs to $\check{\mathrm{C}}_{R_s}(\mathcal{V})$ whenever $\cap_{l=0}^{k} s_{v_l} \neq \emptyset$ and a k-simplex $[v_0, v_1, \cdots, v_k]$ belongs to $\mathcal{R}_{R_c}(\mathcal{V})$ whenever $d(v_l, v_m) \leq R_c$ for all $0 \leq l < m \leq k$. In addition, since we consider only coverage holes on the sphere $\mathbb{S}^2$, it is sufficient to construct 2-dimensional Čech complex and 2-dimensional Rips complex of the WSN, denoted as $\check{\mathrm{C}}^{(2)}_{R_s}(\mathcal{V})$ and $\mathcal{R}^{(2)}_{R_c}(\mathcal{V})$ respectively.

Fig. 2 shows a WSN, its Čech complex and two Rips complexes for two different values of R_c. Depending on the relation of R_c and R_s, the Rips complex and the Čech complex may be close or rather different. In this example, for $R_c = 2R_s$, the Rips complex sees the hole surrounded by $2, 3, 5, 6$ as in the Čech complex whereas it is missed in the Rips complex for $R_c = 2.5R_s$. At the same time, the true coverage hole surrounded by $1, 2, 6$ is missed in both Rips complexes.

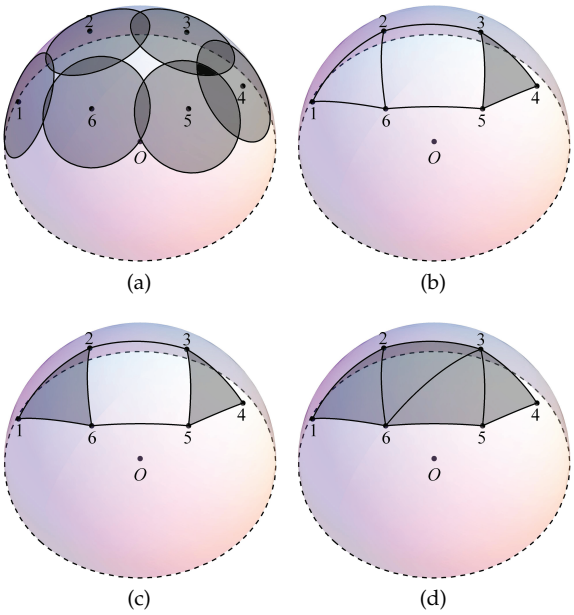

Fig. 2. (a) a WSN, (b) Čech complex, (c) Rips Complex under $R_c = 2R_s$, (d) Rips Complex under $R_c = 2.5R_s$

In fact, as proved in [25], any coverage hole can be found in Čech complex. Furthermore, there are following relations between $\check{\mathrm{C}}^{(2)}_{R_s}(\mathcal{V})$ and $\mathcal{R}^{(2)}_{R_c}(\mathcal{V})$.

Lemma 1. *Let $\mathcal{V}$ denote the set of node locations in a WSN on $\mathbb{S}^2$ with radius R, all nodes have the same sensing radius R_s and communication radius R_c, $R_s \ll R, R_c \ll R$, then*

$$\mathcal{R}^{(2)}_{R_c}(\mathcal{V}) \subset \check{\mathrm{C}}^{(2)}_{R_s}(\mathcal{V}) \subset \mathcal{R}^{(2)}_{2R_s}(\mathcal{V}), \quad \text{whenever } R_c \leq R\arccos([3\cos^2(R_s/R) - 1]/2) \tag{1}$$

Proof. See the Appendix. □

According to (1), some relationships between Čech complex and Rips complex in terms of coverage hole can be derived as illustrated in the following corollaries.

Corollary 1. *When $R_c \leq R\arccos([3\cos^2(R_s/R) - 1]/2)$, if there is no hole in $\mathcal{R}^{(2)}_{R_c}(\mathcal{V})$, there must be no hole in $\check{\mathrm{C}}^{(2)}_{R_s}(\mathcal{V})$.*

Corollary 2. *When $R_c \geq 2R_s$, if there is a hole in $\mathcal{R}^{(2)}_{R_c}(\mathcal{V})$, there must be a hole in $\check{\mathrm{C}}^{(2)}_{R_s}(\mathcal{V})$.*

Corollary 3. *When $R\arccos([3\cos^2(R_s/R) - 1]/2) < R_c < 2R_s$, there is no guarantee relation between $\mathcal{R}^{(2)}_{R_c}(\mathcal{V})$ and $\check{\mathrm{C}}^{(2)}_{R_s}(\mathcal{V})$ in terms of holes.*

From the discussions above, a hole in a $\check{\mathrm{C}}^{(2)}_{R_s}(\mathcal{V})$ not seen in a $\mathcal{R}^{(2)}_{R_c}(\mathcal{V})$ must be bounded by a spherical triangle. Based on this observation, a formal definition of spherical triangular hole is given as follows.

Definition 3 (Spherical triangular hole)**.** *For a pair of complexes $\check{\mathrm{C}}^{(2)}_{R_s}(\mathcal{V})$ and $\mathcal{R}^{(2)}_{R_c}(\mathcal{V})$, a spherical triangular hole is an uncovered region bounded by a spherical triangle (2-simplex) which appears in $\mathcal{R}^{(2)}_{R_c}(\mathcal{V})$ but not in $\check{\mathrm{C}}^{(2)}_{R_s}(\mathcal{V})$.*

4 Bounds on Proportion of Spherical Triangular Holes

In this section, the conditions under which any point on $\mathbb{S}^2$ with radius R is inside a spherical triangular hole are first given. From the discussions in Section 3, it is found that the proportion of the area of spherical triangular holes is related to the relation of R_c and R_s. Three different cases are considered for the proportion computation. For each case, closed-form expressions for lower and upper bounds of the proportion are derived.

4.1 Preliminary

Lemma 2. *For any point on $\mathbb{S}^2$, it is inside a spherical triangular hole if and only if the following two conditions are satisfied:*

1) *the great circle distance between the point and its closest node is larger than R_s.*
2) *the point is inside a spherical triangle: the convex hull of three nodes with pairwise great circle distance less than or equal to R_c.*

Lemma 3. *If there exists a point O which is inside a spherical triangular hole, then $R_s < R\arccos\sqrt{[1 + 2\cos(R_c/R)]/3}$.*

Proof. According to Definition 3, if there is a point O inside a spherical triangular hole, then there exists a 2-simplex $\sigma \in \mathcal{R}^{(2)}_{R_c}(\mathcal{V})$ while $\sigma \notin \check{\mathrm{C}}^{(2)}_{R_s}(\mathcal{V})$, so $\mathcal{R}^{(2)}_{R_c}(\mathcal{V}) \subsetneq \check{\mathrm{C}}^{(2)}_{R_s}(\mathcal{V})$. According to (1), we have $R_c > R\arccos([3\cos^2(R_s/R) - 1]/2) \Rightarrow R_s < R\arccos\sqrt{[1 + 2\cos(R_c/R)]/3}$. □

Lemma 4. *Let O be a point inside a spherical triangular hole and l denote the great circle distance between O and its closest neighbour, then $R_s < l \leq R\arccos\sqrt{[1+2\cos(R_c/R)]/3}$.*

The proof is similar as that of Lemma 1.

Since we assume nodes are distributed on $\mathbb{S}^2$ according to a homogeneous Poisson point process with intensity λ, any point has the same probability to be inside a spherical triangular hole. This probability in a homogeneous setting is also equal to the proportion of the area of spherical triangular holes.

We use spherical coordinates (R,θ,φ) to denote points on $\mathbb{S}^2$ with radius R, where θ is polar angle and φ is azimuth angle. We consider the probability of the point N with spherical coordinates $(R,0,0)$ being inside a spherical triangular hole. Since the communication radius of each sensor is at most R_c, only the nodes within R_c from the point N can contribute to the spherical triangle which bounds a spherical triangular hole containing N. Therefore, we only need to consider the Poisson point process constrained on the spherical cap $C(N,R_c)$ which is also a homogeneous Poisson process with intensity λ, where $C(N,R_c)$ denotes the spherical cap centered at point N and the maximum great circle distance between N and points on the spherical cap is R_c. We denote this process as Φ. In addition, $T(x,y,z)$ denotes the property that the point N is inside the spherical triangular hole bounded by the spherical triangle with points x,y,z as vertices. When n_0,n_1,n_2 are points of the process Φ, $T(n_0,n_1,n_2)$ is also used to denote the event that the spherical triangle formed by the nodes n_0,n_1,n_2 bounds a spherical triangular hole containing the point N. In addition, we use $T'(n_0,n_1,n_2)$ to denote the event that the nodes n_0,n_1,n_2 can not form a spherical triangle which bounds a spherical triangular hole containing the point N.

Let $\tau_0=\tau_0(\Phi)$ be the node in the process Φ which is closest to the point N. There are two cases for the point N to be inside a spherical triangular hole. The first case is that the node τ_0 can contribute to a spherical triangle which bounds a spherical triangular hole containing the point N. The second case is that the node τ_0 can not contribute to any spherical triangle which bounds a spherical triangular hole containing the point N but other three nodes can form a spherical triangle which bounds a spherical triangular hole containing the point N. So the probability that the point N is inside a spherical triangular hole can be defined as

$$\begin{aligned} p(\lambda) &= \mathrm{P}\{N \text{ is inside a spherical triangular hole}\} \\ &= \mathrm{P}\{\bigcup_{\{n_0,n_1,n_2\}\subseteq\Phi} T(n_0,n_1,n_2)\} \\ &= \mathrm{P}\{\bigcup_{\{n_1,n_2\}\subseteq\Phi\setminus\{\tau_0(\Phi)\}} T(\tau_0,n_1,n_2)\} \\ &\quad + \mathrm{P}\{\bigcup_{\substack{\{n_0,\cdots,n_4\}\\ \subseteq\Phi\setminus\{\tau_0(\Phi)\}}} T(n_0,n_1,n_2)\mid T'(\tau_0,n_3,n_4)\} \end{aligned} \tag{2}$$

4.2 Case $0 < R_c \leq R\arccos([3\cos^2(R_s/R)-1]/2)$

Theorem 1. *When $0 < R_c \leq R\arccos([3\cos^2(R_s/R)-1]/2)$, $p(\lambda)=0$.*

Proof. According to (1), when $0 < R_c \leq R\arccos([3\cos^2(R_s/R)-1]/2)$, $\mathcal{R}^{(2)}_{R_c}(\mathcal{V}) \subset \check{\mathrm{C}}^{(2)}_{R_s}(\mathcal{V})$, it means that there exists not a spherical triangle which appears in $\mathcal{R}^{(2)}_{R_c}(\mathcal{V})$ but not in $\check{\mathrm{C}}^{(2)}_{R_s}(\mathcal{V})$, so there is no spherical triangular holes which means $p(\lambda)=0$.

□

4.3 Case $R\arccos([3\cos^2(R_s/R)-1]/2) < R_c \leq 2R_s$

Theorem 2. *When $R\arccos([3\cos^2(R_s/R)-1]/2) < R_c \leq 2R_s$, $p_l(\lambda) < p(\lambda) < p_u(\lambda)$, where*

$$\begin{aligned} p_l(\lambda) &= 2\pi\lambda^2R^4\int_{R_s/R}^{\theta_{0u}}\sin\theta_0 d\theta_0\int_{2\pi-\varphi_m}^{2\varphi_m}d\varphi_1\int_{\theta_0}^{\theta_{1u}}\sin\theta_1 \\ &\quad\times e^{-\lambda|C(N,R\theta_0)|}e^{-\lambda|S^+(\theta_0,\varphi_1)|}(1-e^{-\lambda|S^-(\theta_0,\theta_1,\varphi_1)|})d\theta_1 \end{aligned} \tag{3}$$

and

$$\begin{aligned} p_u(\lambda) &= 2\pi\lambda^2R^4\int_{R_s/R}^{\theta_{0u}}\sin\theta_0 d\theta_0\int_{2\pi-\varphi_m}^{2\varphi_m}d\varphi_1\int_{\theta_0}^{\theta_{1u}}\sin\theta_1 \\ &\quad\times e^{-\lambda|C(N,R\theta_0)|}e^{-\lambda|S^+(\theta_0,\varphi_1)|}(1-e^{-\lambda|S^-(\theta_0,\theta_0,\varphi_1)|})d\theta_1 \\ &\quad+\mathrm{P}\{\bigcup_{\substack{\{n_0,\cdots,n_4\}\\ \subseteq\Phi\setminus\{\tau_0(\Phi)\}}} T(n_0,n_1,n_2)\mid T'(\tau_0,n_3,n_4)\} \end{aligned} \tag{4}$$

and

$$\begin{aligned} \theta_{0u} &= \arccos\sqrt{[1+2\cos(R_c/R)]/3} \\ \varphi_m &= \arccos[(\cos(R_c/R)-\cos^2\theta_0)/(\sin^2\theta_0)] \\ \theta_{1u} &= \min\{\theta_{1u1},\theta_{1u2}\} \\ \theta_{1u1} &= \arccos\frac{\cos(R_c/R)}{\sqrt{1-\sin^2\theta_0\sin^2\varphi_1}}+\arctan(\cos\varphi_1\tan\theta_0) \\ \theta_{1u2} &= \arccos\left[\cos(R_c/R)/\sqrt{1-\sin^2\theta_0\sin^2(\varphi_1-\varphi_m)}\right] \\ &\quad+\arctan(\cos(\varphi_1-\varphi_m)\tan\theta_0) \end{aligned}$$

Proof. We first prove the lower bound. It can be obtained from (2) that

$$p(\lambda) > \mathrm{P}\{\bigcup_{\{n_1,n_2\}\subseteq\Phi\setminus\{\tau_0(\Phi)\}} T(\tau_0,n_1,n_2)\}$$

So for the lower bound, we only consider the first case that the closest node τ_0 must contribute to a spherical triangle which bounds a spherical triangular hole containing the point N.

Using spherical coordinates, we assume the closest node τ_0 lies on $(R,\alpha_0,0)$ and use $|S|$ to denote the area of the set S, then we can get the distribution of α_0 as

$$F_{\alpha_0}(\theta_0)=P(\alpha_0\leq\theta_0)=1-e^{-\lambda|C(N,R\theta_0)|} \tag{5}$$

since the event $\alpha_0>\theta_0$ means that the spherical cap $C(N,R\theta_0)$ does not contain any nodes from the process,

which is given by the Poisson probability $e^{-\lambda|C(N,R\theta_0)|}$. Furthermore, $|C(N,R\theta_0)|$ can be given as

$$|C(N,R\theta_0)| = \int_0^{\theta_0}\int_0^{2\pi} R^2\sin\theta d\varphi d\theta = 2\pi R^2(1-\cos\theta_0) \tag{6}$$

From (5) and (6), we can get the density of τ_0

$$F_{\alpha_0}(d\theta_0) = 2\pi\lambda R^2\sin\theta_0 e^{-\lambda|C(N,R\theta_0)|}d\theta_0 \tag{7}$$

The integration range for θ_0 can be easily obtained. According to Lemma 4, we have $R_s < R\theta_0 \leq R\arccos\sqrt{[1+2\cos(R_c/R)]/3}$, so $R_s/R < \theta_0 \leq \theta_{0u} = \arccos\sqrt{[1+2\cos(R_c/R)]/3}$.

Therefore the probability of the first case can be given as

$$\begin{aligned}&\mathrm{P}\{\bigcup_{\{n_1,n_2\}\subseteq\Phi\setminus\{\tau_0(\Phi)\}} T(\tau_0,n_1,n_2)\}\\ &=\int_{R_s/R}^{\theta_{0u}}\mathrm{P}\{\bigcup_{\{n_1,n_2\}\subseteq\Phi'_{\theta_0}} T((R,\theta_0,0),n_1,n_2)\}F_{\alpha_0}(d\theta_0)\end{aligned} \tag{8}$$

where Φ'_{θ_0} is the restriction of Φ in $C(N,R_c)\backslash C(N,R\theta_0)$.

Once the node τ_0 is determined, the other two nodes must lie in the different half spaces: one in $H^+ = \mathbb{R}^+\times(0,\pi/2)\times(\pi,2\pi)$ and the other in $H^- = \mathbb{R}^+\times(0,\pi/2)\times(0,\pi)$. Assume n_1 lies in H^+ and n_2 lies in H^-. Since the great circle distance to τ_0 is at most R_c, n_1 and n_2 must also lie in the spherical cap $C(\tau_0,R_c)$. Furthermore, the great circle distance to the point N is at most R_c and larger than $R\alpha_0$, they should also lie in the area $C(N,R_c)\backslash C(N,R\alpha_0)$. Therefore, n_1 must lie in $H^+\bigcap C(\tau_0,R_c)\bigcap C(N,R_c)\backslash C(N,R\alpha_0)$ and n_2 must lie in $H^-\bigcap C(\tau_0,R_c)\bigcap C(N,R_c)\backslash C(N,R\alpha_0)$. In addition, considering the great circle distance between n_1 and n_2 should be at most R_c and the point N should be inside the spherical triangle formed by τ_0, n_1 and n_2, n_1 must lie in the shadow area $A^+ = H^+\bigcap C(\tau_0,R_c)\bigcap C(N,R_c)\backslash C(N,R\alpha_0)\bigcap C(M_2,R_c)$, shown in Fig. 3. M_1 and M_2 are two intersection points between bases of spherical caps $C(N,R\alpha_0)$ and $C(\tau_0,R_c)$, such intersection points must exist in this case since $R_c \leq 2R_s < 2R\alpha_0$.

Ordering the nodes in A^+ by increasing azimuth angle so that $\tau_1 = (R,\theta_1,\varphi_1)$ has the smallest azimuth angle φ_1. And assume the nodes τ_0, τ_1 and another node $\tau_2 \in H^-\bigcap C(\tau_0,R_c)\bigcap C(N,R_c)\backslash C(N,R\alpha_0)$ can form a spherical triangle which bounds a spherical triangular hole containing the point N, then τ_2 must lie to the right of the great circle passing through τ_1 and N, denoted by $H^+(\varphi_1)$ which contains all points with azimuth angle $\varphi\in(\varphi_1-\pi,\varphi_1)$. In addition, the great circle distance to τ_1 is no larger than R_c, so the node τ_2 must lie in the region S^-, as illustrated in Fig. 4.

$$\begin{aligned}S^-(\tau_0,\tau_1) = S^-(\alpha_0,\theta_1,\varphi_1) = H^-\bigcap C(\tau_0,R_c)\\ \bigcap C(N,R_c)\backslash C(N,R\theta_0)\bigcap H^+(\varphi_1)\bigcap C(\tau_1,R_c)\end{aligned}$$

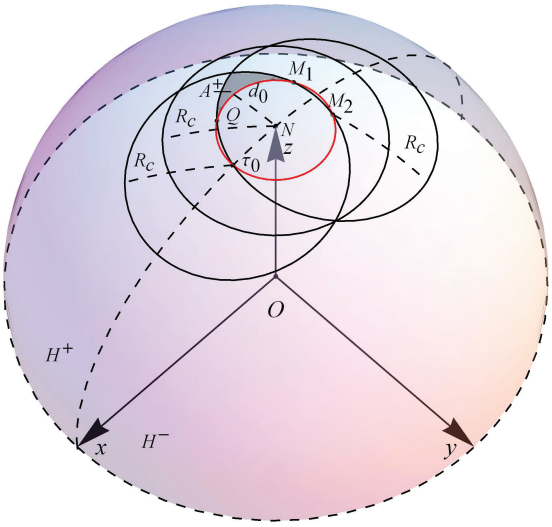

Fig. 3. Illustration of area A^+ in the case $R\arccos([3\cos^2(R_s/R)-1]/2) < R_c \leq 2R_s$

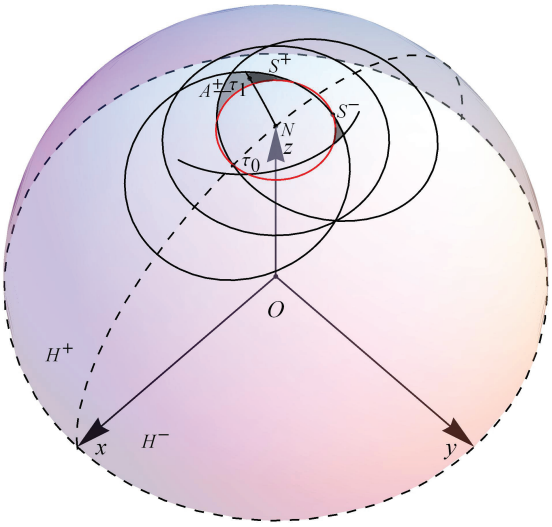

Fig. 4. Illustration of areas S^+ and S^- in the case $R\arccos([3\cos^2(R_s/R)-1]/2) < R_c \leq 2R_s$

Here we need to obtain the density of node τ_1. Considering the way τ_1 was defined, there should be no nodes with a azimuth angle less than φ_1 in A^+, that is to say no nodes are in the region

$$S^+(\tau_0,\tau_1) = S^+(\alpha_0,\varphi_1) = A^+\bigcap H^+(\varphi_1)$$

Since the intensity measure of the Poisson point process in spherical coordinates is $\lambda R^2\sin\theta d\theta d\varphi$, the density F_{τ_1} of τ_1 can be given as

$$F_{\tau_1}(d\theta_1,d\varphi_1) = \lambda R^2\sin\theta_1 e^{-\lambda|S^+(\alpha_0,\varphi_1)|}d\theta_1 d\varphi_1 \tag{9}$$

Then we derive the integration domain $D(\alpha_0)$ with respect to parameters (θ_1,φ_1). Assume the point M_2 has the spherical coordinate $(R,\theta_0,\varphi_m),\varphi_m\in(0,\pi)$. Since the great circle distance between τ_0 and M_2 is

R_c, then according to the spherical law of consines, we have $\cos(R_c/R) = \cos^2\theta_0 + \sin^2\theta_0\cos\varphi_m \Rightarrow \varphi_m = \arccos[(\cos(R_c/R) - \cos^2\theta_0)/(\sin^2\theta_0)]$. It can be seen that points M_1 and Q have the spherical coordinates $(R, \theta_0, 2\pi - \varphi_m)$ and $(R, \theta_0, 2\varphi_m)$ respectively, where Q is one intersection point between bases of spherical caps $C(N, R\alpha_0)$ and $C(M_2, R_c)$. Thus the integration range for φ_1 is $[2\pi - \varphi_m, 2\varphi_m]$. In addition, assume any point with great circle distance R_c to τ_0 has the spherical coordinate (R, θ_t, φ_t), still using the spherical law of consines, we have $\cos(R_c/R) = \cos\theta_0\cos\theta_t + \sin\theta_0\sin\theta_t\cos\varphi_t \Rightarrow \theta_t(\varphi_t) = \arccos[\cos(R_c/R)/\sqrt{1-\sin^2\theta_0\sin^2\varphi_t}] + \arctan(\cos\varphi_t\tan\theta_0)$. Similarly, assume any point with great circle distance R_c to M_2 has the spherical coordinate $(R, \theta_t', \varphi_t')$, we can obtain $\theta_t'(\varphi_t') = \arccos[\cos(R_c/R)/\sqrt{1-\sin^2\theta_0\sin^2(\varphi_t'-\varphi_m)}] + \arctan(\cos(\varphi_t'-\varphi_m)\tan\theta_0)$. Then the integration range for θ_1 is $[\theta_0, \theta_{1u}]$, where $\theta_{1u} = \min\{\theta_{1u1}, \theta_{1u2}\}, \theta_{1u1} = \theta_t(\varphi_1), \theta_{1u2} = \theta_t'(\varphi_1)$. Furthermore, $|S^+(\alpha_0, \varphi_1)|$ can be expressed as

$$|S^+(\alpha_0,\varphi_1)| = \int_{2\pi-\varphi_m}^{\varphi_1}\int_{\alpha_0}^{\theta_{1u}} R^2\sin\theta d\theta d\varphi$$

Assume only τ_0, τ_1 and nodes in $S^-(\tau_0, \tau_1)$ can contribute to the spherical triangle which bounds a spherical triangular hole containing the point N, we can get a lower bound of the probability that the point N is inside a spherical triangular hole. It is a lower bound because it is possible that τ_1 can not contribute to a spherical triangle which bounds a spherical triangular hole containing point N, but some other nodes with higher azimuth angles in the area A^+ can contribute to such a spherical triangle. For example, in Fig. 5, if there is no node in S^- but there are some nodes in S'^-, then τ_1 can not contribute to any spherical triangle which bounds a spherical triangular hole containing point N, but τ_1' can form such a spherical triangle with τ_0 and another node in S'^-. Based on the assumption, we have

$$\begin{aligned}
&\mathrm{P}\{\bigcup_{\{n_1,n_2\}\subseteq\Phi'_{\theta_0}} T((R,\theta_0,0),n_1,n_2)\}\\
&> \mathrm{P}\{\bigcup_{n_2\subseteq\Phi'_{\theta_0}\bigcap S^-(\tau_0,\tau_1)} T((R,\theta_0,0),\tau_1,n_2)\}\\
&= \iint_{D(\theta_0)} \mathrm{P}\{\bigcup_{n_2\subseteq\Phi'_{\theta_0}\bigcap S^-(\theta_0,\theta_1,\varphi_1)} T((R,\theta_0,0),(R,\theta_1,\varphi_1),n_2)\}\\
&\qquad\qquad F_{\tau_1}(d\theta_1,d\varphi_1)\\
&= \iint_{D(\theta_0)} \mathrm{P}\{\Phi'_{\theta_0}(S^-(\theta_0,\theta_1,\varphi_1))>0\}F_{\tau_1}(d\theta_1,d\varphi_1)\\
&= \iint_{D(\theta_0)} (1-e^{-\lambda|S^-(\theta_0,\theta_1,\varphi_1)|})F_{\tau_1}(d\theta_1,d\varphi_1)
\end{aligned} \tag{10}$$

where $|S^-(\theta_0, \theta_1, \varphi_1)|$ can be expressed as

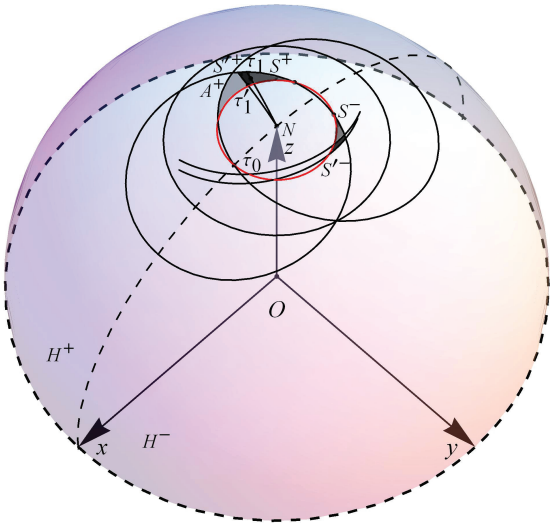

Fig. 5. Illustration of areas S'^+ and S'^- in the case $R\arccos([3\cos^2(R_s/R)-1]/2) < R_c \le 2R_s$

$$|S^-(\theta_0,\theta_1,\varphi_1)| = \int_{\varphi_{2l}}^{\varphi_m}\int_{\theta_0}^{\theta_{2u}} R^2\sin\theta_2 d\theta_2 d\varphi_2 \tag{11}$$

and

$$\begin{aligned}
\varphi_{2l} &= \varphi_1 - \arccos\frac{\cos(Rc/R)-\cos\theta_1\cos\theta_0}{\sin\theta_1\sin\theta_0}\\
\theta_{2u} &= \min\{\theta_{1u1},\theta_{2u2}\}\\
\theta_{2u2} &= \arccos\Big[\cos(R_c/R)/\sqrt{1-\sin^2\theta_0\sin^2(\varphi_2-\varphi_1)}\Big]\\
&\quad + \arctan(\cos(\varphi_2-\varphi_1)\tan\theta_1)
\end{aligned}$$

Therefore, from (7), (8), (9) and (10), the lower bound shown in (3) can be derived.

Next we will prove the upper bound. As discussed in Section 4.1, there are two cases for the point N being inside a spherical triangular hole. As for the second case that the closest node τ_0 can not but some other nodes can contribute to a spherical triangle which bounds a spherical triangular hole containing the point N, it is not easy to obtain a closed-form expression for such probability, but we can get it by simulations. Simulation results show that this probability is less than 0.16% whenever $R_c \le 3R_s$ with any intensity λ. So we still focus on the probability of the first case.

For the lower bound, we only considered the case that τ_1 contributes to a spherical triangle which bounds a spherical triangular hole containing point N. For the upper bound, we need to further consider the case that τ_1 can not but some other nodes in A^+ can contribute to such a spherical triangle, shown in Fig. 5. Assume the node $\tau_1' = (R, \theta_1', \varphi_1')$ with the second smallest azimuth angle in A^+ can contribute to such a spherical triangle, it means that there is no node in $S^-(\alpha_0, \theta_1, \varphi_1)$ but there is at least one node in the region $S'^-(\alpha_0, \theta_1, \varphi_1, \theta_1', \varphi_1') = S^-(\alpha_0, \theta_1', \varphi_1')\backslash S^-(\alpha_0, \theta_1, \varphi_1)$.

Then the density of the pair (τ_1, τ_1') is given as

$$F_{\tau_1,\tau_1'}(d\theta_1, d\varphi_1, d\theta_1', d\varphi_1') = \lambda^2 R^4 \sin\theta_1 \sin\theta_1' e^{-\lambda|S^+(\alpha_0,\varphi_1')|} d\theta_1 d\varphi_1 d\theta_1' d\varphi_1' \tag{12}$$

The probability that τ_1 can not but τ_1' can form a spherical triangle which bounds a spherical triangular hole containing point N with τ_0 and another node in $S'^-(\alpha_0, \theta_1, \varphi_1, \theta_1', \varphi_1')$ can be given as

$$\begin{aligned}
&\mathrm{P}\{\bigcup_{\substack{\{n_3,n_4\}\subseteq\Phi'_{\theta_0}\\ \bigcap S^-(\tau_0,\tau_1')}} T((R,\theta_0,0),\tau_1',n_4) \mid T'((R,\theta_0,0),\tau_1,n_3)\} \\
&= \iiiint \mathrm{P}\{\Phi'_{\theta_0}(S^-(\theta_0,\theta_1,\varphi_1)) = 0\} \\
&\qquad \times \mathrm{P}\{\Phi'_{\theta_0}(S'^-(\theta_0,\theta_1,\varphi_1,\theta_1',\varphi_1')) > 0\} \\
&\qquad F_{\tau_1,\tau_1'}(d\theta_1, d\varphi_1, d\theta_1', d\varphi_1') \\
&= \iiiint e^{-\lambda|S^-(\theta_0,\theta_1,\varphi_1)|} \times (1 - e^{-\lambda|S'^-(\theta_0,\theta_1,\varphi_1,\theta_1',\varphi_1')|}) \\
&\qquad F_{\tau_1,\tau_1'}(d\theta_1, d\varphi_1, d\theta_1', d\varphi_1')
\end{aligned} \tag{13}$$

As we can see from Fig. 5, as long as τ_1' has a higher polar angle than τ_1 has, the sum of $|S^-(\alpha_0,\theta_1,\varphi_1)|$ and $|S'^-(\alpha_0,\theta_1,\varphi_1,\theta_1',\varphi_1')|$ will be always smaller than $|S^-(\alpha_0,\alpha_0,\varphi_1)|$.

Therefore we can get from (13)

$$\begin{aligned}
&\mathrm{P}\{\bigcup_{\substack{\{n_3,n_4\}\subseteq\Phi'_{\theta_0}\\ \bigcap S^-(\tau_0,\tau_1')}} T((R,\theta_0,0),\tau_1',n_4) \mid T'((R,\theta_0,0),\tau_1,n_3)\} \\
&< \iiiint (e^{-\lambda|S^-(\theta_0,\theta_1,\varphi_1)|} - e^{-\lambda|S^-(\theta_0,\theta_0,\varphi_1)|}) \\
&\qquad F_{\tau_1,\tau_1'}(d\theta_1, d\varphi_1, d\theta_1', d\varphi_1')
\end{aligned} \tag{14}$$

Let $S'^+(\theta_0,\varphi_1,\varphi_1') = S^+(\theta_0,\varphi_1')\backslash S^+(\theta_0,\varphi_1)$, then

$$\begin{aligned}
&\iint \lambda R^2 \sin\theta_1' e^{-\lambda|S'^+(\theta_0,\varphi_1,\varphi_1')|} d\theta_1' d\varphi_1' \\
&\qquad = 1 - e^{-\lambda|A^+\backslash S^+(\theta_0,\varphi_1)|} < 1
\end{aligned} \tag{15}$$

It is the complement of the probability that no node is in the area $A^+\backslash S^+(\theta_0,\varphi_1)$.

From (10), (12), (14) and (15), we can obtain

$$\begin{aligned}
&\mathrm{P}\{\bigcup_{n_2\subseteq\Phi'_{\theta_0}\bigcap S^-(\tau_0,\tau_1)} T((R,\theta_0,0),\tau_1,n_2)\} \\
&+ \mathrm{P}\{\bigcup_{\substack{\{n_3,n_4\}\subseteq\Phi'_{\theta_0}\\ \bigcap S^-(\tau_0,\tau_1')}} T((R,\theta_0,0),\tau_1',n_4) \mid T'((R,\theta_0,0),\tau_1,n_3)\} \\
&< \iint_{D(\theta_0)} (1 - e^{-\lambda|S^-(\theta_0,\theta_0,\varphi_1)|}) F_{\tau_1}(d\theta_1, d\varphi_1)
\end{aligned} \tag{16}$$

where $|S^-(\theta_0,\theta_0,\varphi_1)|$ has the similar expression as (11).

Similarly, we can further consider the case that neither of τ_1 and τ_1' can contribute to a spherical triangle which bounds a spherical triangular hole containing point N, but other nodes with even higher azimuth angle can contribute to such a spherical triangle. In this way, we can get the same result as (16).

Therefore, it can be derived that

$$\begin{aligned}
&\mathrm{P}\{\bigcup_{\{n_1,n_2\}\subseteq\Phi'_{\theta_0}} T((R,\theta_0,0),n_1,n_2)\} \\
&< \iint_{D(\theta_0)} (1 - e^{-\lambda|S^-(\theta_0,\theta_0,\varphi_1)|}) F_{\tau_1}(d\theta_1, d\varphi_1)
\end{aligned} \tag{17}$$

From (2), (7), (8), (12) and (17), the upper bound shown in (4) can be derived.

□

4.4 Case $R_c > 2R_s$

Theorem 3. *When $R_c > 2R_s$, $p_l(\lambda) < p(\lambda) < p_u(\lambda)$, where*

$$\begin{aligned}
p_l(\lambda) = 2\pi\lambda^2 R^4 \Big\{ &\int_{\frac{R_s}{R}}^{\frac{R_c}{2R}} \sin\theta_0 d\theta_0 \int_\pi^{2\pi} d\varphi_1 \int_{\theta_0}^{\theta'_{1u}} \sin\theta_1 \\
&\times e^{-\lambda|C(N,R\theta_0)|} e^{-\lambda|S^+(\theta_0,\varphi_1)|} (1 - e^{-\lambda|S^-(\theta_0,\theta_1,\varphi_1)|}) d\theta_1 \\
&+ \int_{R_c/2R}^{\theta_{0u}} \sin\theta_0 d\theta_0 \int_{2\pi-\varphi_m}^{2\varphi_m} d\varphi_1 \int_{\theta_0}^{\theta_{1u}} \sin\theta_1 e^{-\lambda|C(N,R\theta_0)|} \\
&\times e^{-\lambda|S^+(\theta_0,\varphi_1)|} (1 - e^{-\lambda|S^-(\theta_0,\theta_1,\varphi_1)|}) d\theta_1 \Big\}
\end{aligned} \tag{18}$$

and

$$\begin{aligned}
p_u(\lambda) = 2\pi\lambda^2 R^4 \Big\{ &\int_{\frac{R_s}{R}}^{\frac{R_c}{2R}} \sin\theta_0 d\theta_0 \int_\pi^{2\pi} d\varphi_1 \int_{\theta_0}^{\theta'_{1u}} \sin\theta_1 \\
&\times e^{-\lambda|C(N,R\theta_0)|} e^{-\lambda|S^+(\theta_0,\varphi_1)|} (1 - e^{-\lambda|S^-(\theta_0,\theta_0,\varphi_1)|}) d\theta_1 \\
&+ \int_{R_c/2R}^{\theta_{0u}} \sin\theta_0 d\theta_0 \int_{2\pi-\varphi_m}^{2\varphi_m} d\varphi_1 \int_{\theta_0}^{\theta_{1u}} \sin\theta_1 e^{-\lambda|C(N,R\theta_0)|} \\
&\times e^{-\lambda|S^+(\theta_0,\varphi_1)|} (1 - e^{-\lambda|S^-(\theta_0,\theta_0,\varphi_1)|}) d\theta_1 \Big\} \\
&+ \mathrm{P}\{\bigcup_{\substack{\{n_0,\cdots,n_4\}\\ \subseteq\Phi\backslash\{\tau_0(\Phi)\}}} T(n_0,n_1,n_2) \mid T'(\tau_0,n_3,n_4)\}
\end{aligned} \tag{19}$$

and

$$\begin{aligned}
\theta'_{1u} &= \min\{\theta_{1u1}, \theta'_{1u2}\} \\
\theta'_{1u2} &= \arccos\Big[\cos(R_c/R)/\sqrt{1 - \sin^2\theta_0 \sin^2(\varphi_1 - \pi)}\Big] \\
&\quad + \arctan(\cos(\varphi_1 - \pi)\tan\theta_0)
\end{aligned}$$

In this case, we can use the same method as in Section 4.3 to get the lower and upper bounds, shown in (18) and (19) respectively. But we need to consider two situations $R_s/R < \theta_0 \le R_c/(2R)$ and $R_c/(2R) < \theta_0 \le \theta_{0u} = \arccos\sqrt{[1 + 2\cos(R_c/R)]/3}$. In the first situation, $\theta_0 \le R_c/(2R)$ means that the spherical cap $C(N, R\theta_0)$ is completely included in the spherical cap $C(\tau_0, R_c)$. The illustrations for the areas A^+, S^+, S^-, S'^+ and S'^- are shown in Fig. 6(a) and 6(b) respectively. In addition, the integration range for φ_1 is $[\pi, 2\pi]$. The second situation is the same as that in Section 4.3.

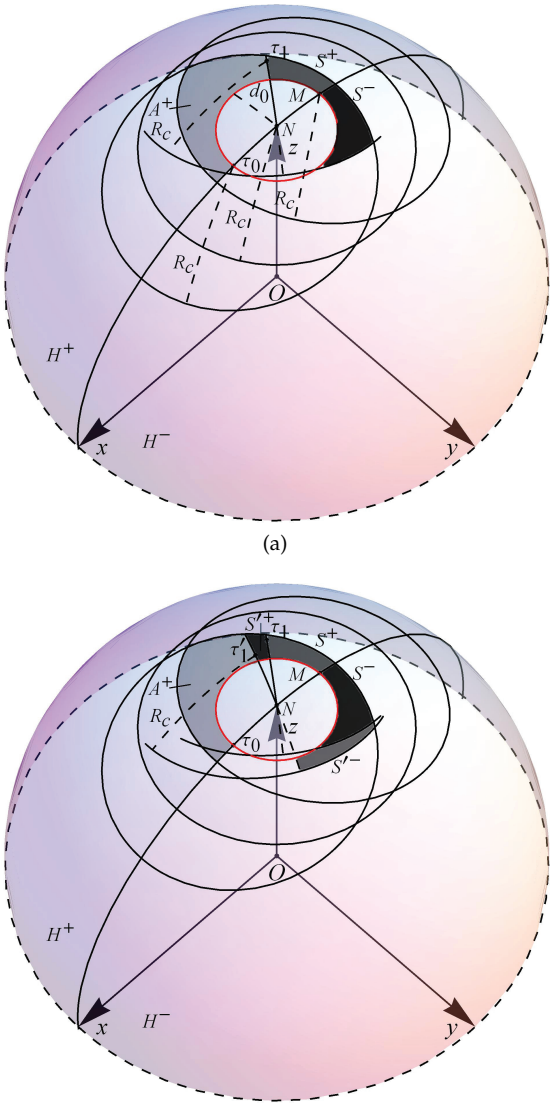

Fig. 6. Illustrations of areas in case $R_c > 2R_s$. (a) the areas A^+, S^+ and S^- (b) the areas S'^+ and S'^-

5 Simulations and Performance Evaluation

In this section, simulation settings are first given. Then simulation results are compared with analytical lower and upper bounds under different settings of R_s, R_c, R.

5.1 Simulation settings

A sphere centered at the origin with radius R is considered in the simulations. The probability of the point with spherical coordinate $(R, 0, 0)$ being inside a spherical triangular hole is computed. Sensors are randomly distributed on the sphere according to a homogeneous Poisson point process with intensity λ. The sensing radius R_s of each node is set to be 10 meters and communication radius R_c is chosen from 20 to 30 meters with interval of 2 meters. Let $\gamma = R_c/R_s$, then γ ranges from 2 to 3 with interval of 0.2. In addition, λ is selected from 0.001 to 0.020 with interval of 0.001. For each pair of (λ, γ), 10^7 simulations are run to check whether the point with spherical coordinate $(R, 0, 0)$ belongs to a spherical triangular hole.

5.2 Impact of R_s and R_c

As illustrated in Section 3, $R_s \ll R$ and $R_c \ll R$, here we choose $R = 10R_s$ to analyse the impact of R_s and R_c on the probability of any point being inside a spherical triangular hole. Under this configuration, the probability $p(\lambda)$ obtained by simulations is presented with the lower and upper bounds in Fig. 7(a) and 7(b) respectively.

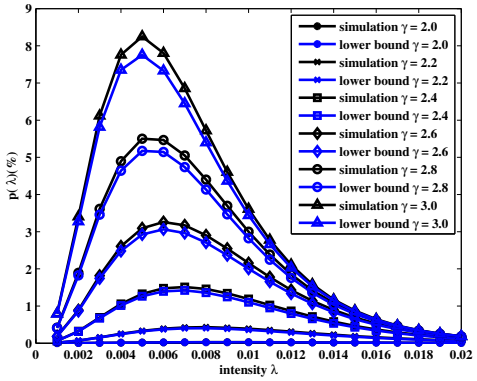

(a)

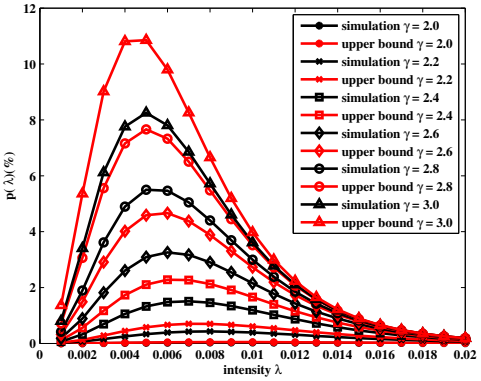

(b)

Fig. 7. Proportion of the area of spherical triangular holes under $R = 10R_s$ (a) simulation results and lower bounds ; (b) simulation results and upper bounds

It can be seen that for any value of γ, $p(\lambda)$ has a maximum at a threshold value λ_c of the intensity. As a matter of fact, for $\lambda \leq \lambda_c$, the number of nodes is small. Consequently the probability of any point being inside a spherical triangular hole is relatively small too. With the increase of λ, the connectivity between nodes becomes stronger. As a result, the probability of any point being inside a spherical triangular hole increases. However, when the intensity reaches the threshold value, the probability is up to its maximum. $p(\lambda)$ decreases for $\lambda \geq \lambda_c$. The simulations also show that λ_c decreases with the increase of γ.

On the other hand, it can be seen from Fig. 7(a) and 7(b) that for a fixed intensity λ, $p(\lambda)$ increases with the increases of γ. That is because when R_s is fixed, the larger R_c is, the higher is the probability of each spherical triangle containing a coverage hole.

Furthermore, the maximum probability increases quickly with γ ranging from 2.0 to 3.0. These results can also provide some insights for planning of WSNs, which will be discussed in Section 5.4.

Finally, it can be found in Fig. 7(a) that the probability obtained by simulation is very well consistent with the lower bound. The maximum difference between them is about 0.5%. Fig. 7(b) shows that probability obtained by simulation is also consistent with the upper bound. The maximum difference between them is about 3%.

5.3 Impact of R

Although we assume $R_s \ll R$ and $R_c \ll R$, to better understand the impact of R on the probability of any point being inside a spherical triangular hole, we choose R to be $5R_s, 10R_s$ and $100R_s$. In addition, we also want to know the difference of the probability under spherical and 2D planar cases. Therefore, simulation results, lower and upper bounds of the probability under spheres with radii $5R_s, 10R_s, 100R_s$ and 2D plane are shown in Fig. 8(a), 8(b) and 8(c) respectively.

It can be seen from Fig. 8 that simulations results, lower and upper bounds under spheres with radii $5R_s, 10R_s, 100R_s$ and 2D plane are very close with each other. More precisely, the maximum difference of simulations results under spheres with radii $5R_s$ and $10R_s$ is about 0.045%, which is about 0.06% under spheres with radii $5R_s$ and $100R_s$ and is about 0.03% under spheres with radii $10R_s$ and $100R_s$. In addition, the maximum differences of simulation results between 2D planar case and spherical cases with radii $5R_s, 10R_s, 100R_s$ are 0.05%, 0.03% and 0.02% respectively. It means the larger the radius of sphere is, the more closer are the simulation results under sphere and 2D plane, it is because the larger the radius of sphere is, the more likely of the local of each node on the sphere to be planar.

With respect to lower and upper bounds, it is found that under any two spheres with radii $5R_s, 10R_s, 100R_s$, the maximum difference of lower and upper bounds are 0.06% and 0.12% respectively. Furthermore, under spheres with radii $5R_s, 10R_s, 100R_s$ and 2D plane, the maximum difference of lower bounds is also 0.06%, and that of upper bounds is also 0.12%. More importantly, under sphere with radius $100R_s$ and 2D plane, the maximum difference of lower bounds is 5×10^{-6} and that of upper bounds is 2.5×10^{-5}. It means the probabilities under cases of sphere with radius $100R_s$ and 2D plane are nearly the same, which is quite logical since when the radius of sphere is much more larger than the sensing radius of any node, the local of any node can be considered to be planar.

It can be further found that under above cases, the maximum differences of simulation results, lower and upper bounds are all so small that they can be neglected. Consequently, it also means that the radius of sphere has little impact on the probability of any point on the sphere to be inside a spherical triangular hole. Our results can thus be extended to more general 3D surfaces.

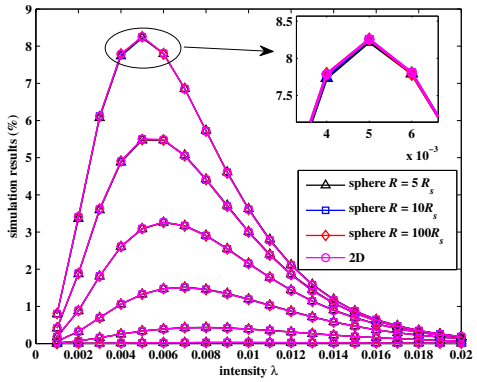

(a)

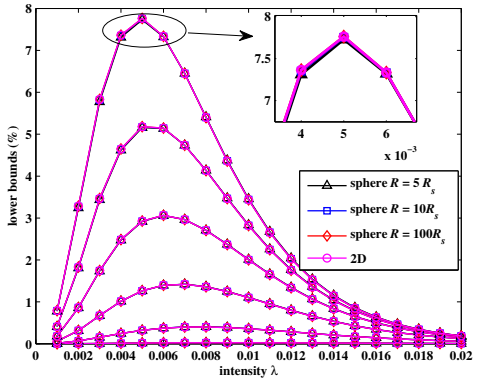

(b)

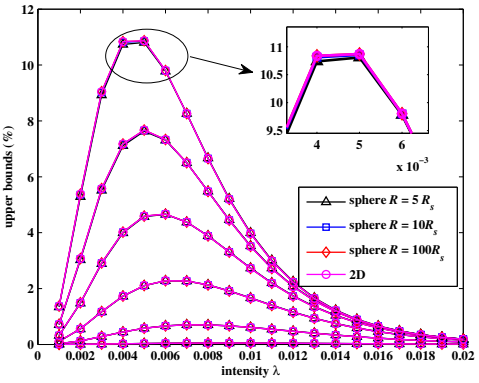

(c)

Fig. 8. Comparison of the proportion of the area of spherical triangular holes (a) comparison of simulation results; (b) comparison of lower bounds; (c) comparison of upper bounds

5.4 Discussions on applications

In this paper, we only consider spherical triangular holes, for non-spherical triangular holes, we assume they can be detected and covered by additional nodes. Under this assumption, our analytical results can be used for planning of WSNs. For example, a WSN is used to monitor a mountain and the ratio $\gamma = 2$, according to the analytical upper bounds, we can see that the maximum proportion of the area of spherical triangular holes under $\gamma = 2$ is about 0.06 %, which can be neglected. It means that as long as the surface of mountain can be spherically triangulated by nodes, we can say the mountain is covered. But if $\gamma = 3$ and at least 95% of the surface of the mountain should be covered, then it means that the proportion of the area of spherical triangular holes can be at most 5%. From the analytical upper bounds of $\gamma = 3$, it can be seen that when the intensity $\lambda = 0.009$, the upper bound is about 5%, so in order to cover at least 95% of the mountain, the intensity of nodes should be larger than 0.009. Similarly, our results can also be used in the scenarios when using satellite to cover the whole earth.

6 Conclusion

This paper studied the accuracy of homology-based coverage hole detection for wireless sensor networks on sphere. First, the situations when Rips complex may miss coverage holes were identified. Then we chose the proportion of the area of coverage holes missed by Rips complex as a metric to evaluate the accuracy. Three different cases were considered to compute the accuracy. For each case, closed-form expressions for lower and upper bounds were derived. Simulation results are well consistent with the derived lower and upper bounds, with maximum differences of 0.5% and 3% respectively. In addition, simulation results also show that the radius of sphere has little impact on the accuracy as long as it is much larger than communication and sensing radii of each sensor. This means that our results can be applied to more general 3D surfaces although the results are derived on sphere. This problem will be investigated in our future work.

Appendix
Proof of Lemma 1

Proof. The second inclusion is trivial because for any k-simplex $[v_0, v_1, \cdots, v_k] \in \check{\mathrm{C}}^{(2)}_{R_s}(\mathcal{V})$, it means the sensing ranges of these nodes have a common intersection, so the pairwise distance $d(v_i, v_j) \leq 2R_s$ for all $0 \leq i < j \leq k$, which means $[v_0, v_1, \cdots, v_k] \in \mathcal{R}^{(2)}_{2R_s}(\mathcal{V})$.

As for the first inclusion, it is clear that $\mathcal{R}^{(2)}_{R_c}(\mathcal{V})$ and $\check{\mathrm{C}}^{(2)}_{R_s}(\mathcal{V})$ contain the same 0-simplices. It is also easy to see that all 1-simplices in $\mathcal{R}^{(2)}_{R_c}(\mathcal{V})$ must also be in $\check{\mathrm{C}}^{(2)}_{R_s}(\mathcal{V})$ since for any 1-simplex $[v_i, v_j]$ with distance $d(v_i, v_j) \leq R_c \leq R\arccos([3\cos^2(R_s/R) - 1]/2) < R\arccos(2\cos^2(R_s/R) - 1) = 2R_s$, it means that the sensing ranges of the two nodes have a common intersection. So we only need to prove that all 2-simplices in $\mathcal{R}^{(2)}_{R_c}(\mathcal{V})$ must be in $\check{\mathrm{C}}^{(2)}_{R_s}(\mathcal{V})$. It is equivalent to say that for any three nodes with pairwise great circle distance no larger than R_c, their sensing ranges must have a common intersection.

Assume a 2-simplex $[v_0, v_1, v_2] \in \mathcal{R}^{(2)}_{R_c}(\mathcal{V})$, then the three nodes v_0, v_1 and v_2 must determine a plane α. We consider the spherical cap on $\mathbb{S}^2$ cut off by the plane α. Since $R_c < R$, the spherical cap must be on a hemisphere. It is easy to see that the intersection of the plane α and sphere $\mathbb{S}^2$ is a circle c. Let O_1 be the center of circle c, O be the center of $\mathbb{S}^2$, P be the intersection of line OO_1 and $\mathbb{S}^2$.

Using spherical coordinates, we assume the point P has a spherical coordinate $(R, 0, 0)$. P may be inside[1] or outside the spherical triangle $v_0v_1v_2$, which is shown in Fig. 9(a) and 9(b) respectively.

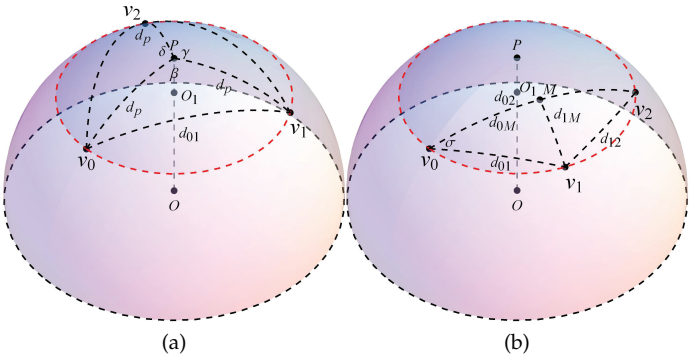

Fig. 9. Illustrations of P and spherical triangle $v_0v_1v_2$: (a) P is inside the spherical triangle $v_0v_1v_2$; (b) P is outside the spherical triangle $v_0v_1v_2$.

It can be seen that P has the same great circle distance to v_0, v_1 and v_2, denoted by d_p. If P is inside the spherical triangle $v_0v_1v_2$, as shown in Fig. 9(a), then we can prove $d_p \leq R_s$. Since P lying inside the spherical triangle $v_0v_1v_2$ means $\beta + \gamma + \delta = 2\pi$, there must be one angle no smaller than $2\pi/3$. Without loss of generality, assume $\beta \geq 2\pi/3$. According to the spherical law of consines, we have $\cos(\beta) = \frac{\cos(d_{01}/R) - \cos^2(d_p/R)}{\sin^2(d_p/R)} \leq -1/2 \Rightarrow \cos(d_{01}/R) \leq [3\cos^2(d_p/R) - 1]/2$. In addition, $d_{01} \leq R_c \leq R\arccos([3\cos^2(R_s/R) - 1]/2) \Rightarrow \cos(d_{01}/R) \geq [3\cos^2(R_s/R) - 1]/2$, and $0 < d_{01}/R, d_p/R < \pi/2$, so we have $[3\cos^2(R_s/R) - 1]/2 \leq [3\cos^2(d_p/R) - 1]/2 \Rightarrow d_p \leq R_s$, which means the point P is a common intersection of sensing ranges of v_0, v_1 and v_2, so $[v_0, v_1, v_2] \in \check{\mathrm{C}}^{(2)}_{R_s}(\mathcal{V})$.

If P is outside the spherical triangle $v_0v_1v_2$, as shown in Fig. 9(a), it indicates that the spherical triangle $v_0v_1v_2$ must be contained in half of the spherical cap. Assume v_0, v_1 and v_2 have spherical coordinates $(R, \theta, \varphi_0), (R, \theta, \varphi_1)$ and (R, θ, φ_2), where $\theta \in$

1. It also includes the case that P is on one arc of the spherical triangle $v_0v_1v_2$.

$(0, \pi/2), \varphi_0 < \varphi_1 < \varphi_2$, then we have $\varphi_1 - \varphi_0, \varphi_2 - \varphi_1, \varphi_2 - \varphi_0 \in (0, \pi)$. Using d_{01}, d_{12}, d_{02} to denote the pairwise great circle distances between v_0, v_1, v_2, then according to the spherical law of consines, we have

$$\cos(d_{01}/R) = \cos^2\theta + \sin^2\theta\cos(\varphi_1 - \varphi_0) \quad (20)$$

$$\cos(d_{12}/R) = \cos^2\theta + \sin^2\theta\cos(\varphi_2 - \varphi_1) \quad (21)$$

$$\cos(d_{02}/R) = \cos^2\theta + \sin^2\theta\cos(\varphi_2 - \varphi_0) \quad (22)$$

In addition, we use σ to denote the angle between two arcs $\widehat{v_0v_1}$ and $\widehat{v_0v_2}$, M to denote the middle point of the arc $\widehat{v_0v_2}$ and d_{0M}, d_{1M} to denote great circle distances between v_0, v_1 and M. It can be seen $d_{0M} = d_{02}/2$. Similarly, we have

$$\cos\sigma = \frac{\cos(d_{12}/R) - \cos(d_{01}/R)\cos(d_{02}/R)}{\sin(d_{01}/R)\sin(d_{02}/R)} \quad (23)$$

$$\cos\frac{d_{1M}}{R} = \cos\frac{d_{01}}{R}\cos\frac{d_{0M}}{2R} + \sin\frac{d_{01}}{R}\cos\frac{d_{0M}}{2R}\cos\sigma \quad (24)$$

From (23) and (24), we can obtain

$$\cos\frac{d_{1M}}{R} = \frac{\cos(d_{01}/R) + \cos(d_{12}/R)}{2\cos(d_{02}/(2R))} \quad (25)$$

Consequently

$$\cos\frac{d_{1M}}{R} - \cos\frac{d_{0M}}{R} = \frac{\cos\frac{d_{01}}{R} + \cos\frac{d_{12}}{R} - \cos\frac{d_{02}}{R} - 1}{2\cos(d_{02}/(2R))} \quad (26)$$

From (20), (21), (22) and (26), we get

$$\cos\frac{d_{1M}}{R} - \cos\frac{d_{0M}}{R} = \frac{\sin^2\theta\cos\frac{\varphi_2-\varphi_0}{2}\sin\frac{\varphi_1-\varphi_0}{2}\sin\frac{\varphi_2-\varphi_1}{2}}{\cos\frac{d_{02}}{2R}} \quad (27)$$

Since $0 < \varphi_1 - \varphi_0, \varphi_2 - \varphi_1, \varphi_2 - \varphi_0 < \pi$ and $0 < d_{1M}/R, d_{0M}/R, d_{02}/R < \pi/2$, it can be obtained from (27) $d_{1M} < d_{0M} \leq R_c/2 < R_s$, which means the point M is a common intersection of the sensing ranges of v_0, v_1 and v_2, so $[v_0, v_1, v_2] \in \check{\mathrm{C}}^{(2)}_{R_s}(\mathcal{V})$. It means all 2-simplices in $\mathcal{R}^{(2)}_{R_c}(\mathcal{V})$ must be in $\check{\mathrm{C}}^{(2)}_{R_s}(\mathcal{V})$. Consequently the first inclusion is proved.

□

REFERENCES

[1] Q. Fang, J. Gao, and L. Guibas, "Locating and bypassing routing holes in sensor networks," in *Proc. IEEE INFOCOM*, vol. 4, Hong Kong, China, Mar. 2004, pp. 2458–2468.

[2] G. Wang, G. Cao, and T. La Porta, "Movement-assisted sensor deployment," in *Proc. IEEE INFOCOM*, vol. 4, Hong Kong, China, Mar. 2004, pp. 2469–2479.

[3] C. Zhang, Y. Zhang, and Y. Fang, "Localized algorithms for coverage boundary detection in wireless sensor networks," *Wirel. Netw.*, vol. 15, no. 1, pp. 3–20, Jan. 2009.

[4] C. Huang and Y. Tseng, "The coverage problem in a wireless sensor network," in *Proc. ACM WSNA*, San Diego, California, USA, Sep. 2003, pp. 115–121.

[5] C.-F. Huang, Y.-C. Tseng, and L.-C. Lo, "The coverage problem in three-dimensional wireless sensor networks," in *Proc. IEEE Globecom*, vol. 5, Dallas, Texas, Dec. 2004, pp. 3182 – 3186.

[6] Y. Bejerano, "Simple and efficient k-coverage verification without location information," in *Proc. IEEE INFOCOM*, Phoenix, Arizona, USA, Apr. 2008, pp. 897–905.

[7] ——, "Coverage verification without location information," *IEEE Trans. Mobile Comput.*, vol. 11, no. 4, pp. 631–643, Apr. 2012.

[8] H. Zhou, S. Xia, M. Jin, and H. Wu, "Localized algorithm for precise boundary detection in 3d wireless networks," in *Proc. IEEE ICDCS*, Genova, Italy, Jun. 2010, pp. 744–753.

[9] V. de Silva, R. Ghrist, and A. Muhammad, "Blind swarms for coverage in 2-d," in *Proc. Robotics: Science and Systems*, Cambridge, MA, Jun. 2005, pp. 335–342.

[10] V. de Silva and R. Ghrist, "Coverage in sensor networks via persistent homology," *Algebraic & Geometric Topology*, vol. 7, pp. 339–358, 2007.

[11] R. Ghrist and A. Muhammad, "Coverage and hole-detection in sensor networks via homology," in *Proc. 4th International Conference on Information Processing in Sensor Networks*, Los Angeles, California, USA, Apr. 2005, pp. 254–260.

[12] B. Liu and D. Towsley, "A study of the coverage of large-scale sensor networks," in *Proc. IEEE MASS*, Fort Lauderdale, Florida, USA, Oct. 2004, pp. 475–483.

[13] L. Lazos and R. Poovendran, "Stochastic coverage in heterogeneous sensor networks," *ACM Trans. Sen. Netw.*, vol. 2, no. 3, pp. 325–358, Aug. 2006.

[14] P.-J. Wan and C.-W. Yi, "Coverage by randomly deployed wireless sensor networks," *IEEE Trans. Inf. Theory*, vol. 52, no. 6, pp. 2658–2669, Jun. 2006.

[15] X. Li, D. K. Hunter, and S. Zuyev, "Coverage properties of the target area in wireless sensor networks," *IEEE Trans. Inf. Theory*, vol. 58, no. 1, pp. 430–437, Jan. 2012.

[16] M.-C. Zhao, J. Lei, M.-Y. Wu, Y. Liu, and W. Shu, "Surface coverage in wireless sensor networks," in *Proc. IEEE INFOCOM*, Rio de Janeiro, Brazil, Apr. 2009, pp. 109 –117.

[17] L. Liu and H. Ma, "On coverage of wireless sensor networks for rolling terrains," *IEEE Trans. Parallel Distrib. Syst.*, vol. 23, no. 1, pp. 118 –125, Jan. 2012.

[18] F. Yan, P. Martins, and L. Decreusefond, "Accuracy of homology based approaches for coverage hole detection in wireless sensor networks," in *Proc. IEEE ICC*, Ottawa, Canada, Jun. 2012.

[19] A. Muhammad and M. Egerstedt, "Control using higher order laplacians in network topologies," in *Proc. 17th International Symposium on Mathematical Theory of Networks and Systems*, Kyoto, Japan, Jul. 2006, pp. 1024–1038.

[20] A. Muhammad and A. Jadbabaie, "Decentralized computation of homology groups in networks by gossip," in *Proc. American Control Conference*, New York, NY, USA, Jul. 2007, pp. 3438–3443.

[21] A. Tahbaz-Salehi and A. Jadbabaie, "Distributed coverage verification in sensor networks without location information," *IEEE Trans. Autom. Control*, vol. 55, no. 8, pp. 1837–1849, Aug. 2010.

[22] M. A. Armstrong, *Basic Topology*. Springer, 1983.

[23] J. Munkres, *Elements of algebraic topology*. Addison-Wesley, 1984.

[24] A. Hatcher, *Algebraic Topology*. Camebridge University Press, 2002.

[25] R. Bott and L. W. Tu, *Differential Forms in Algebraic Topology*. Springer-Verlag, 1982.

Feng Yan received the B.S. degree from Huazhong University of Science and Technology, China, in 2005 and the M.S. degree from Southeast University, China, in 2008, both in electrical engineering. He is currently pursuing the Ph.D degree in the Network and Computer Science Department, at Telecom ParisTech, Paris, France. His current research interests are in the areas of wireless communications and wireless networks, with emphasis on applications of homology theory in wireless networks.

Philippe Martins received a M.S. degree in signal processing and another M.S. degree in networking and computer science from Orsay University and ESIGETEL France, in 1996. He received the Ph.D. degree with honors in electrical engineering from Telecom ParisTech, Paris, France, in 2000.

He is currently a Professor in the Network and Computer Science Department, at Telecom ParisTech. His main research interests lie in performance evaluation in wireless networks (RRM, scheduling, handover algorithms, radio metrology). His current investigations address mainly three issues: a) the design of distributed sensing algorithms for cognitive radio b) distributed coverage holes detection in wireless sensor networks c) the definition of analytical models for the planning and the dimensioning of cellular systems. He has published several papers on different international journals and conferences. He is also an IEEE senior member and he is co-author of several books on 3G and 4G systems.

Laurent Decreusefond is a former student of Ecole Normale Supérieure de Cachan. He obtained his Ph.D. degree in Mathematics in 1994 from Telecom ParisTech and his Habilitation in 2001. He is currently a Professor in the Network and Computer Science Department, at Telecom ParisTech. His main fields of interest are the Malliavin calculus, the stochastic analysis of long range dependent processes, random geometry and topology and their applications. With P. Moyal, he co-authored a book about the stochastic modelling of telecommunication systems.